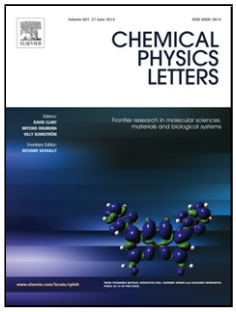

Title: Photoinduced coupled twisted intramolecular charge transfer and excited-state proton transfer via intermolecular hydrogen bonding: a DFT/TD-DFT study

Author: Dandan Wang Rui Lü Minghu Yuan Junsheng Chen Liqiang Feng Aiping Fu Fenghui Tian António J.C. Varandas Tianshu Chu

PII: S0009-2614(14)00587-9
DOI: http://dx.doi.org/doi:10.1016/j.cplett.2014.07.012
Reference: CPLETT 32325

To appear in:

Received date: 18-3-2014
Revised date: 3-7-2014
Accepted date: 4-7-2014

Please cite this article as: D. Wang, R. Lü, M. Yuan, J. Chen, L. Feng, A. Fu, F. Tian, A.J.C. Varandas, T. Chu, Photoinduced coupled twisted intramolecular charge transfer and excited-state proton transfer via intermolecular hydrogen bonding: a DFT/TD-DFT study, *Chem. Phys. Lett.* (2014), http://dx.doi.org/10.1016/j.cplett.2014.07.012

Graphical Abstract

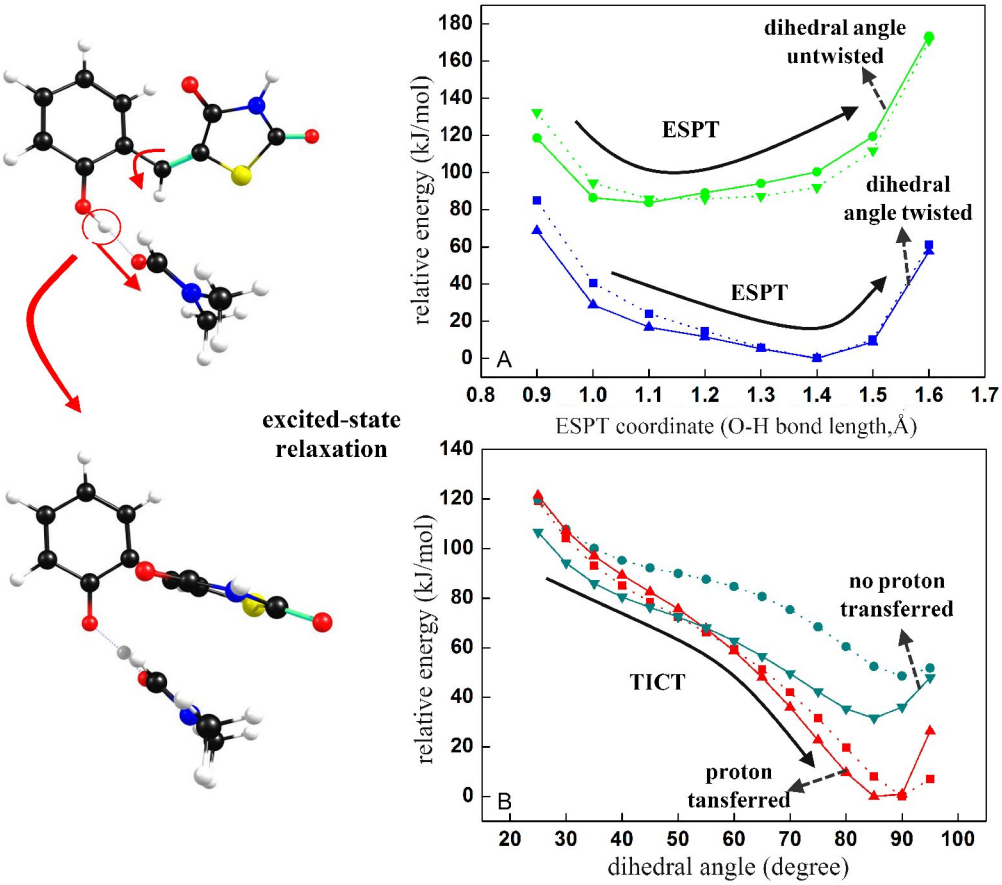

Highlights

- The DFT/TD-DFT investigation on the photoinduced coupled TICT and ESPT.
- The ESPT is induced by the intermolecular hydrogen-bond strengthening.
- The early occurred TICT facilitates the ESPT.
- The coupling of TICT and ESPT is energetically preferable.
- A verification calculation is performed at the CC2/def-TZVP level.

Photoinduced coupled twisted intramolecular charge transfer and excited-state proton transfer via intermolecular hydrogen bonding: a DFT/TD-DFT study

Dandan Wang,[1] Rui Lü,[2] Minghu Yuan,[1] Junsheng Chen,[1] Liqiang Feng,[1] Aiping Fu,[3] Fenghui Tian,[3] António J.C. Varandas[4*] and Tianshu Chu,[1,3*]

[1]State Key Laboratory of Molecular Reaction Dynamics, Dalian Institute of Chemical Physics, Chinese Academy of Sciences, Dalian, 116023, People's Republic of China
[2] Laboratory of Pathogenic Biology, Medical College, Qingdao University, Qingdao, 266071, People's Republic of China
[3]Institute for Computational Sciences and Engineering, Laboratory of New Fiber Materials and Modern Textile, the Growing Base for State Key Laboratory, Qingdao University, Qingdao, 266071, People's Republic of China
[4]Departamento de Química and Centro de Química, Universidade de Coimbra, 3004-535 Coimbra, Portugal

Abstract

We discuss theoretically the geometric and electronic structure properties of the thiazolidinedione derivative A and its hydrogen-bonded complex in dimethylformamide (DMF) solution in the S_0 and S_1 states. To gain insight into the photoinduced coupled excited-state proton transfer (ESPT) and twisted intramolecular charge transfer (TICT) associated with intermolecular hydrogen bonding, the potential energy profiles are provided along the O—H bond and the twisted angle. It is predicted that TICT in S_1 can facilitate ESPT initiated by intermolecular hydrogen-bond strengthening in the S_1 state. The coupling of ESPT and TICT is energetically preferable.

Key words: time-dependent density functional theory; hydrogen bonding dynamics; photoexcitation; twisted intramolecular charge transfer (TICT); excited-state proton transfer (ESPT).

*Corresponding authors, Emails: tschu@dicp.ac.cn; tschu008@163.com; varandas@uc.pt

1. Introduction

The site-specific hydrogen bonding interaction usually plays a significant role in many photochemical and photophysical processes [1-12]. Upon photoexcitation, molecules in chemistry and biology can undergo excited-state proton transfer (ESPT) associated with hydrogen bond accepting and donating abilities [13-15]. Specifically, it has been demonstrated that ground-state proton transfer (PT) and/or ESPT via hydrogen bonding are essential to unravel complex problems, such as the mechanism of proton-relay processes in biological systems, transport proton in water, mutagenesis and molecular recognition [16-22], etc. In fact, PT and ESPT can be enhanced or restrained by intermolecular and/or intramolecular hydrogen-bonding interactions [23-29]. On the other hand, upon photoexcitation, charge redistribution usually occurs in molecules and it has been proved that conformational twist of molecules can dramatically enhance the charge transfer process. Indeed, considering a photoinduced charge-transfer process in one molecule where the electron donor and acceptor are linked via a single bond or a bridge subunit, that is, intramolecular charge transfer (ICT), both the planar intramolecular charge transfer (PICT) and the twisted intramolecular charge transfer (TICT) may occur in the excited state [30-33]. This suggests that, for large conjugated systems or donor-acceptor models, intramolecular charge transfer in the excited state may be accompanied with concomitant rotation of subunits [34-37]. A number of studies have revealed that the TICT in the excited state is also responsible for the novel dual fluorescence phenomenon [38, 39]. Meanwhile, Malval *et al.* has demonstrated that coupling of TICT with ESPT may occur in

gradually twisted donor-acceptor phenol-pyridinium biphenyl series [38]. However, although much work has been performed either on the twisted intramolecular charge transfer or the excited intramolecular proton transfer [13-15, 30-33], few has focused on the correlation of the ESPT and the conformational twist. In fact, little has been done on ultrafast excited-state proton transfer coupled by conformational twisting in excited state. Both of these two processes may be driven by charge rearrangement in excited state and coupling between them may contribute to special or novel photochemical and photophysical properties. Clearly, further efforts are welcomed in this area.

In the present work, we have found that the above two crucial processes can take place simultaneously and cooperatively in the newly synthesized thiazolidinedione derivative A (TZD-A) in dimethylformamide (DMF) solution [40]. The TZDs are excellent hydrogen bond host-guest complexes, and most importantly, in TZD-A, the electron donor (D) and acceptor (A) are linked by a single bond without bulk steric effect, which can easily lead to the confirmation twist in both the ground and the excited states. Additionally, due to potential intramolecular charge transfer through the single bond between the electron donor and acceptor, the structural and energetic relaxation in the excited state may be distinct from the ground state. Taking the above into account, we have established a model to illustrate the correlation between TICT and ESPT in detail by studying TZD-A in dimethylformamide. And based on the density functional theory (DFT) and time-dependent DFT (TD-DFT) calculations, a relatively new and detailed mechanism is unravelled concerning the TICT and ESPT

processes and the hydrogen bonding dynamics in the excited state. Further, high level *ab initio* calculations with the second-order approximate coupled-cluster (CC2) method are carried out to check and validate our results from DFT calculation.

2. Theoretical method

The ground-state structures were optimized using DFT [41, 42] and the first-excited-state structures were optimized using TD-DFT [43]. Vibrational frequencies at the optimized structures were calculated to ensure that the obtained configurations correspond to local minima on the ground and excited states. The Becke's three-parameter hybrid exchange-correlation functional of Coulomb-attenuating, CAM-B3LYP [44, 45], was used in the DFT calculations for both the ground- and excited-states, in order to suitably describe the intermolecular charge transfer (ICT) in the excited state, an issue that is largely involved in the present study. All optimizations and energy calculations employed the 6-311G+(d,p) basis set and were carried out with the Gaussian 09 program suite [46]. Besides, our preliminary test on basis sets has demonstrated that the 6-311G+(d,p) basis set is suitable for studying the present system by giving calculation results in good agreement with the experimental ones.

In the calculation of the absorption spectra solvent effect were included using the integral equation formalism (IEF) version of polarizable continuum model [47,48] (PCM) with the dielectric constant of n,n-dimethylformamide (ε=37.22).

To check the TD-DFT results, the potential energy profiles of the first-excited state were further calculated at the *ab initio* level by use of the second-order approximate coupled-cluster method [49, 50]. All CC2 calculations were carried out using the basis set def-TZVP, which offer high computational efficiency without sacrificing the accuracy [51]. They have all been performed with the TRUBOMOLE-6.3 program package [52].

3. Results and discussion

3.1 Geometric and electronic properties of ground- and first-excited states by TD-DFT calculations

The equilibrium geometric structures of the hydrogen-bonded complex A-DMF in the ground (S_0) and in the first excited (S_1) state are shown in Figure 1, together with the geometric parameters of bond length and dihedral angle. All local minima have been confirmed to have real frequencies from the vibrational frequency analysis. We note here that there is only one local minimum in the S_1 state of A-DMF. As shown, the distance between O3 and H7 is 0.981 Å and 1.409 Å for the ground- and first-excited states, respectively. The distance between H7 and O4 is shortened from 1.720 Å in S_0 to 1.053 Å in S_1 and the bond length C3—O3 is shortened from 1.347 Å in S_0 to 1.258 Å in S_1 while the bond length C11=O4 is lengthened from 1.226 Å in S_0 to 1.273 Å in S_1. Upon photoexcitation, the dihedral angle between the thiazolidinedione and the aryl ring (C1-C2-C7-C8), changes from 33.46º to 87.40º, indicating that the thiazolidinedione ring is almost perpendicular to the aryl ring in the

S_1 state. Besides these important parameters, the bond lengths change significantly in the DMF moiety, the thiazolidinedione ring and the aryl ring due to photoexcitation. Hence, photoexcitation exerts a key effect on the structural configuration of the hydrogen-bonded A-DMF complex.

The electronic spectra have been obtained using TD-DFT for TZD-A (in S_0 state) and A-DMF (in S_0 state), with the results being collected in Table 1. First, for S_1 state and compared with TZD-A, the vertical electronic spectrum of A-DMF shows a redshift of 9 nm that is induced by the intermolecular hydrogen bonding interaction, and the strong absorption peaks of the TZD-A and A-DMF are predicted to both appear in the S_1 state. Then, for S_2, the excitation energy is decreased from 297 nm/4.18 eV in TZD-A to 298 nm/4.16 eV in A-DMF. Table 1 also lists the contribution of the orbital transitions to the two low-lying electronic states. It shows that the transition from HOMO (highest-occupied molecular orbital) to LUMO (lowest-unoccupied molecular orbital) is the dominant orbital contribution for the S_1 state and the transition from HOMO-1 to LUMO is the dominant one for the S_2 state in both TZD-A and A-DMF. Additionally, the electronic spectrum (i.e. the emission spectrum) of the S_1 equilibrium structure of A-DMF is also shown in Table 1. As seen, the first excited state emission peak of A-DMF is located at 952nm, and this demonstrates that the S_1 state of A-DMF yields no fluorescence. Hence, the one obvious fluorescence peak at 424nm in the experimental work in Ref. [40] can be ascribed to the monomer TZD-A, because the calculated fluorescence emission peak at 389 nm of TZD-A agrees with that of the experiment. Figure 2 illustrates the

calculated absorption spectra of TZD-A and A-DMF, showing clearly a spectral redshift for the latter complex. Here, the theoretical absorption peaks and the spectral redshift of 9nm all agree reasonably with the experimental results. We further note that there are very little changes in the obtained spectra after consideration of solvent effect in the calculation, i.e., the absorption peak changes from 326nm (without solvent effect) to 327nm (with solvent effect) in TZD-A, and from 335nm to 336nm in A-DMF.

Figure 3 shows the frontier orbitals of TZD-A (monomer, in S_0 state) and A-DMF (dimer, in S_0 state). Obviously, the S_1 state is a $\pi\pi^*$ state, the electron density is delocalized over the TZD-A moiety in A-DMF. Furthermore, the charge transfer occurs from the aryl moiety to the thiazolidinedione moiety in the HOMO-LUMO transition and the electron density of the C3—O3 group is decreased in LUMO as compared with that in HOMO. Thus, the S_1 state of A-DMF shows intramolecular charge transfer (ICT) character, and simultaneously the hydrogen bond O3—H7···O4=C11 becomes strengthened in the first excited state. Additionally, comparing the frontier orbitals between TZD-A and A-DMF, one can find that the presence of intermolecular hydrogen-bonding restrains intramolecular charge transfer from the aryl to the thiazolidinedione moiety, thus suggesting that conformational twist generated by the ICT state is not so easy to occur with the presence of the intermolecular hydrogen-bonding. Similarly, the S_2 state shows the characteristic of an ICT state based on the analysis of the frontier orbitals especially the transition from HOMO-1 to LUMO. In addition, the frontier orbitals for S_1 equilibrium structure of

A-DMF were also calculated and shown in Figure 3. Comparing with S_0 equilibrium structure, the ICT character of S_1 equilibrium structure becomes more distinct, with the electron density completely moved from aryl to the thiazolidinedione moiety. This suggests that the intramolecular charge transfer is more preferable in the more twisted excited-state structure.

The net charge distribution in the atoms of A-DMF in the S_0 and S_1 states is shown in Table 2, together with the charge difference between the two electronic states and the dipole moments. And the charge changes of the electron donor and acceptor have also been marked on Figure 3. Clearly, the large dipole moment of the S_1 state also suggests a charge-transfer character. In the first excited state, the net charge distribution in the atoms of the thiazolidinedione moiety generally becomes more negative, as compared with the ground state. But the net charge distribution in the atoms of the aryl moiety tends to be more positive when A-DMF is photoexcited from the ground- to the first-excited states. From the above analysis, it is clear that photoexcitation of A-DMF has caused charge transfer from the aryl to the thiazolidinedione moiety. Furthermore, the net charge distribution in O3 of A-DMF changes from -0.311 in S_0 to -0.550 in S_1, thus indicating that the hydrogen bond involving the O3 atom is strengthened in the excited state. To summarize, the agreement is satisfactory between the analyses of molecular orbitals and the net charge distribution.

3.2 Potential energy surface profiles of the first-excited state by TD-DFT

calculations

The potential energy curves along the different reaction coordinates (i.e., the distance between O3 and H7, and the twisted dihedral angle) are considered and calculated here for the first excited electronic state of A-DMF using the TD-DFT/CAM-B3LYP method. The corresponding results are firstly shown in Figure 4. Like one construction method reported in Ref. [53] for potential energy profiles for the excited-state proton transfer, the present potential energy curves in Figure 4A have been obtained by rigid abstraction of the hydrogen atom of the O3—H7 group. Thus, all internal coordinates, except the O3—H7 distance, have been kept fixed in these calculations. Likewise, in Figure 4B, the potential energy curves are constructed by changing the dihedral angle between the aryl and the thiazolidinedione ring (C1-C2-C7-C8), while the other coordinates are constrained and fixed.

Four kinds of curves are shown in Figure 4, corresponding to four typical cuts of the potential energy surface of the S_1 state. Potential curve P1-a in Figure 4A shows a profile of A-DMF in S_1 as a function of the O3—H7 distance when the dihedral angle (C1-C2-C7-C8) is kept unchanged (33.46°). According to the optimized equilibrium geometry of A-DMF, the configuration with this fixed dihedral angle of 33.46° and the bond length O3—H7 of 0.9 Å should be taken as the geometry of the reactant, while the optimized proton transfer geometry in S_1 without configuration twist is taken as the product in this case. Below, we use the 'relative energy' to denote the 'potential energy' because the energy shown in the figure has taken the minimum energy of the two curves (P1 and P2, or, P3 and P4) as the reference zero energy and

thus it has a relative value. Although the relative energy of the complex is predicted to decrease when changing the O3—H7 distance from 0.9 Å to 1.1 Å, however, the relative energy rises up drastically and steeply when the O3—H7 bond length is varied from 1.1 Å to 1.6 Å, implying that ESPT is unfavorable without configuration twist between the aryl and the thiazolidinedione ring. In other words, a hindrance is encountered to the ESPT process in the absence of TICT.

Potential curve P2-a in Figure 4A shows the corresponding energy profile of A-DMF, which is also a function of the O3—H7 distance but with dihedral angle (C1-C2-C7-C8) being kept to be 87.40°. Here, the presently optimized TICT geometry in the S_1 state is taken as the product. One observes that the relative energy drops dramatically by increasing the O—H bond length until reaching the local minimum. This demonstrates that the ESPT process is barrierless and thus is much easier to take place with dihedral angle (C1-C2-C7-C8) being twisted to 87.40º.

Potential curve P3-a in Figure 4B illustrates the relative energy versus the dihedral angle, with the O3—H7 distance fixed at 1.409 Å (note that the ESPT process should already occur with such O3—H7 distance value). Here, the product is the equilibrium geometry of the TICT state. Seen in this figure, the energy drops monotonically with the increasing dihedral angle. This demonstrates that it is till energetically preferable even if the TICT process occurs after the ESPT process. However, among the four potential curves in Figure 4, this third curve P3-a has the highest energy at the initial point, suggesting that an earlier occurrence of the ESPT process than the TICT process is not so energetically favorable.

Potential curve P4-a in Figure 4B shows the relative energy versus the dihedral angle (C1-C2-C7-C8), with the O3—H7 distance fixed at 0.981 Å. The structure corresponding to the initial geometry in this case, is shown in Figure 5, where the dihedral angle (C1-C2-C7-C8) and bond length O3—H7 are 25° and 0.981 Å, on the basis of the optimized equilibrium geometry of A-DMF. Unlike the potential curve P1-a, the relative energy in P4-a decreases fast to the local minimum with no barrier, giving an indication that the TICT is much more favorable than ESPT in S_1 from the vertical excitation point. This may infer that TICT tends to occur early and primarily in the S_1 state and then activates the ESPT in the S_1 state.

To gain more insight into the coupled TICT and ESPT in the S_1 state, we further compare the potential curve of P1-a with that of P2-a (see Figure 4A), and the potential curve of P3-a with that of P4-a (see Figure 4B). Through this approach, the energy difference can be well quantified under the different reaction pathways. In Figure 4A, the energy gap between the two potential curves becomes large with the increase in the O3—H7 distance and no "intersection" is found, thus indicating that the TICT lowers the energy significantly. That is to say, TICT is energetically advantageous. In Figure 4B, there is one "intersection" between the P3-a and the P4-a potential energy curves, which is estimated to occur at the twisted dihedral angle of 55°. How such distinct cuts of the potential energy surface actually communicate with each other is an interesting issue that requires further investigation. But here it is sufficient to anticipate that the two processes are likely to cooperate with each other tightly, either alternately or in parallel.

Figure 5 shows the configurations of the initial points of the four potential energy curves, denoted as P1-1, P2-1, P3-1 and P4-1, together with the local minimum geometries on the four potential energy curves, denoted as P1-2, P2-2, P3-2 and P4-2. Note here that P2-2 and P3-2 have the same geometry.

To help understanding the coupled ESPT and TICT processes and the coupling mechanism between them, we show, in Figure 6, the relative energies corresponding to the three critical geometries of P1-2, P2-2 (P3-2) and P4-2. As noted before, P1-2 is the structure corresponding to the local minimum on the P1-a potential energy curve. This structure has a very high relative energy, which makes the sole ESPT in the A-DMF complex not so easy to occur in the excited S_1 state. From further comparison with the relative energies of the twisted geometries in the S_1 state, it can be revealed that the twisting behavior further lowers the energy of the complex, resulting in a relatively more stable structure P4-2. Most significantly, it can be seen that the coupling of the ESPT with the TICT process leads to the most stable structure P2-2 (P3-2) which is energetically preferable.

3.3 Potential energy surface profiles of the first-excited state by CC2 calculation: verification of the TD-DFT calculation

The corresponding potential energy curves at CC2/def-TZVP level (labeled with -b) have been presented in Figure 4, for comparison with those at CAM-B3LYP/6-311G+(d,p) level (labeled with –a). In Figure 4A, clearly, the potential energy curve of P1-b and P2-b gives similar shape and tendency to that of P1-a and P2-a, and both P2-b and P2-a has the same local minimum at the O3—H7 distance of 1.4 Å. In Figure 4B, the local minimum of P4-b lies at dihedral angle=90º,

which is faintly different from that of P4-a. Most significantly, the coupling of the ESPT and TICT processes is predicted to be much more energetically favorable by the CC2 calculation, because the P3-b potential curve lies completely below P4-b with no "intersection" between them. Also, in Figure 6, the energy tendency of the three critical geometries is seen to be similar from the two methods. Thus, the qualitatively good agreement, between the DFT and the CC2 methods in the comparative study of the first excited-state potential energy surface profiles, supports the reliability of the conclusive presumption from the DFT calculations about the coupled TICT and ESPT processes. Additionally, it should be noted that, for legible visualization, the two curves from the CC2 (P1-b and P2-b, or, P3-b and P4-b) and the DFT (P1-a and P2-a, or, P3-a and P4-a) calculations in each sole picture of Figure 4, have taken the energy of their own local minimum in the excited state as the reference zero energy. And there also has a similar situation in Figure 6. Actually, the calculated single point energy from the CC2 method is about 2.4 a.u. higher than that from the TDDFT method, but this has completely no influence on the conclusions drawn from a comparative view point of the energies.

4. Conclusions

In this work, the geometric and electronic properties of the ground as well as the low-lying excited singlet states of the thiazolidinedione derivative A and its hydrogen-bonded A-DMF complex have been theoretically studied via DFT and TD-DFT calculations with CAM-B3LYP functional. The relatively strong hydrogen bonding formed between thiazolidinedione derivative A and dimethylformamide in the ground state is found to be strengthened in the first excited state, with the hydrogen-bonded complex showing an intense tendency to transfer the proton of the

thiazolidinedione moiety to DMF. Upon photoexcitation, the proton is transferred to DMF from the O3 atom of thiazolidinedione moiety via intermolecular hydrogen bonding, and a configuration twist between the thiazolidinedione ring and the aryl ring also takes place in the S_1 state. Molecular frontier orbitals and net charge distribution analyses indicate that the S_1 state has obvious ICT character. It has also been found that the coupling of the two important ESPT and TICT processes is beneficial in stabilizing the total energy of A-DMF in the S_1 state. TICT is shown to be able to facilitate the process of ESPT in the first excited state by lowering the energy, while the earlier occurrence of ESPT seems not to be energetically favorable. It is thus further predicted that TICT occurs earlier than ESPT in the S_1 state, with the coupling between them then following. Hence, the present work may useful for enhancing our understanding of the coupled ESPT and TICT processes with the regulation of the excited-state hydrogen bonding dynamics. Finally, we note that Sobolewski and Domcke [54] have showed that with increasing CT character, the TD-DFT method systematically underestimates the energy of a molecular system when compared with the MRMP2 method. Therefore, to moderately correct such TD-DFT drawback, here we have adopted the CAM-B3LYP functional, which is shown to be able to give improved results [55]. In addition, for a better and accurate understanding of the present issue, further calculation with *ab initio* method without this drawback, i.e., the CC2 calculation with def-TZVP basis set, has been carried out to construct the first excited-state potential energy curves and then compared with the TD-DFT/CAM-B3LYP results. This comparison serves to validate and buttress the

reliability of those conclusions drawn from the TD-DFT calculations.

Acknowledgements

This work is supported by the National Natural Science Foundation of China under the grant nos. 21273234, 21103096 and 20833008. AJCV thanks FEDER through "Programa Operacional Factores de Competitividade - COMPETE" and national funds under the auspices of Fundação para a Ciência e a Tecnologia, Portugal, for financial support.

References

[1] K.L. Han, G.J. Zhao, Hydrogen bonding and transfer in the excited state, John Wiley & Sons Ltd, Chichester UK, 2011.

[2] J.B. Asbury, T. Steinel, C. Stromberg, K.J. Gaffney, I.R. Piletic, A. Goun, M.D. Fayer, Phys. Rev. Lett. 91 (2003) 237402.

[3] A.W. Acton, A.D. Allen, L.M. Antunes, J. Am. Chem. Soc. 124 (2002) 13790.

[4] K.L. Han and G.Z. He, J. Photochem. Photobiol. C: Photochem. Rev. 8 (2007) 55.

[5] A.C. Benniston, A. Harriman, Chem. Soc. Rev. 35 (2006) 169.

[6] A.S.D. Sandanayaka, H. Sasabe, T. Takata, O. Ito, J. Photochem. Photobiol. C 11 (2010) 73.

[7] D.D Wang, G.J. Zhao, Commun. Comput. Chem. 2 (2013) 181.

[8] G.J. Zhao, K.L. Han, J. Phys. Chem. A 113 (2009) 4788.

[9] G.J. Zhao, K.L. Han, Biophys. J. 94 (2008) 38.

[10] G.J. Zhao, K.L. Han, P.J. Stang, J. Chem. Theory Comput. 5 (2009) 1955.

[11] G.J. Zhao, B.H. Northrop, P.J. Stang, K.L. Han, J. Phys. Chem. A 114 (2010) 3418.

[12] G.J. Zhao, K.L. Han, Acc. Chem. Res. 45 (2012) 404.

[13] M. Kasha, J. Chem. Soc. Faraday Trans. 2 82 (1986) 2379.

[14] J. Waluk in: J. Waluk (ed.), Conformational Analysis of Molecules in Excited States, Wiley-VCH, New York, 2000, p. 57.

[15] J. Waluk, Acc. Chem. Res. 36 (2003) 832.

[16] Proton Transfer in Biological Systems, Special issue of Frontiers in Bioscience，2003, 8.

[17] M. Tuckerman, K. Laasonen, M. Sprik, M. Parrinello, J. Phys. Chem. 99 (1995) 5749.

[18] D. Marx, M.E. Tuckerman, J. Hutter, M. Parrinello, Nature (London) 397 (1999) 601.

[19] P.L. Geissler, C. Dellago, D. Chandler, J. Hutter, M. Parrinello, Science 291 (2001) 2121.

[20] M.F. Goodman, Nature (London) 378 (1995) 237.

[21] M. Meuwly, A. Mueller, S. Leutwyler, Phys. Chem. Chem. Phys. 5 (2003) 2663.

[22] H.C. Chou, C.H. Hsu, Y.M. Cheng, C.C. Cheng, H.W. Liu, S.C. Pu, P.T. Chou, J. Am. Chem. Soc. 126 (2004) 1650.

[23] G.J. Zhao, J.Y. Liu, L.C. Zhou, K.L. Han, J. Phys. Chem. B 111 (2007) 8940.

[24] K.L. Han, J.D. Huang, S. Chai, S.H. Wen and W.Q. Deng, Nat. Prot. Exch., 2013, DOI: 10.1038/protex.2013.070.

[25] F.B.Yu, P.Li, B.S. Wang, K.L. Han, J. Am. Chem. Soc. 135 (2013) 7674.

[26] A.L. Sobolewski, W. Domcke, Eur. Phys. J. D. 20 (2002) 369.

[27] A. Schaäfer, C. Huber, R. Ahlrichs, J. Chem. Phys. 100 (1994) 5829.

[28] P.T. Chou, C.H. Huang, S.C. Pu, Y.M. Cheng, Y.H. Liu, Y. Wang, C.T. Chen, J. Phys. Chem. A 108 (2004) 6452.

[29] P.T. Chou, S.C. Pu, Y.M. Cheng, W.S. Yu, Y.C. Yu, F.T. Hung, W.P. Hu, J. Phys. Chem. A 109 (2005) 3777.

[30] Z.R. Grabowski, K. Rotkiewicz, W. Rettig, Chem. Rev. 103 (2003) 3899.

[31] M.X. Zhang, G.J. Zhao, ChemSusChem 5 (2012) 879.

[32] C.J. Jödicke, H.P. Lüthi, J. Am. Chem. Soc. 125 (2003) 252.

[33] X. Xu, Z. Cao, Q. Zhang, J. Chem. Phys. 122 (2005) 194305.

[34] E.C. Brown, T.J. Marks, M.A. Ratner, J. Phys. Chem. B 112 (2008) 44.

[35] R. Zalesny, W. Bartkowiak, S. Styrcz, J. Leszczynski, J. Phys. Chem. A 106 (2002) 4032.

[36] A. Boeglin, A. Barsella, A. Fort, M. Mançois, V. Rodriguez, V. Diemer, H.

Chaumeil, A. Defoin, P. Jacques, C. CarréOptical, Chem. Phys. Lett. 442 (2007) 298.

[37] W. Rettig, Angew. Chem. Int. Ed. Engl. 25 (1986) 971.

[38] J.P. Malval, V. Diemer, F. Morlet-Savary, P. Jacques, H. Chaumeil, A. Defoin, C. Carre, O. Poizat, J. Phys. Chem. A 114 (2010) 2401.

[39] S.I. Druzhinin, B.D. Bursulaya, B.M. Uzhinov, J. Photochem. Photobio. A 90 (1995) 53.

[40] A. Sarkar, P. Banerjee, S.U. Hossain, S. Bhattacharya, S.C. Bhattacharya, Spectrochim. Acta. Part A 72 (2009) 1097.

[41] N. Blouin, A. Michaud, D. Gendron, S. Wakim, E. Blair, R. Neagu-Plesu, M. Belleteête, G. Durocher, Y. Tao, M. Leclerc, J. Am. Chem. Soc. 130 (2008) 732−742.

[42] N. Leclerc, A. Michaud, K. Sirois, J.F. Morin, M. Leclerc, Adv. Funct. Mater. 16 (2006) 1694.

[43] R.E. Stratmann, G.E. Scuseria, M.J. Frisch, J. Chem. Phys. 109 (1998) 8218.

[44] A.D. Becke, J. Chem. Phys. 98 (1993) 5648.

[45] T. Yanai, D.P. Tew, N.C. Handy, Chem. Phys. Lett. 393 (2004) 51.

[46] http://www.gaussian.com/g_prod/g09.htm.

[47] S. Miertuš, E. Scrocco, J. Tomasi, Chem. Phys. 55 (1981) 117.

[48] R. Cammi, J. Tomasi, J. Comput. Chem. 16 (1995) 1449.

[49] C. Hätting, J. Chem. Phys. 118 (2003) 7751.

[50] A. Köhn, C. Hätting, J. Chem. Phys. 119 (2003) 5021.

[51] A. Schafer, C. Huber, R. Ahlrichs, J. Chem. Phys. 100 (1994) 5829.

[52] R. Ahlrichs, M. Bär, H. Horn, C. Kölmel, Chem. Phys. Lett. 162 (1989) 165.

[53] A.L. Sobolewski, W. Domcke, J. Phys. Chem. A 111 (2007) 11725.

[54] A.L. Sobolewski, W. Domcke, Chem. Phys. 294 (2003) 73.

[55] D. Jacquemin, E.A. Perpete, G. Scalmani, M.J. Frisch, R. Kobayashi and C. Adamo, J. Chem. Phys. 126 (2007) 144105.

Table 1. Calculated electronic spectra for TZD-A and its hydrogen-bonded A-DMF complex.

	TZD-A(S_0)		A-DMF (S_0)[d]		A-DMF (S_1)[e]	
	E (nm/eV)	*f*	*E* (nm/eV)	*f*	*E* (nm/eV)	*f*
S_1	326/3.80[b]	0.3762	335/3.70	0.3788	952/1.30	0.0002
S_1-cont.[a]	HOMO—L UMO (93%)[c]		HOMO—LUMO (96%)		HOMO—LUMO (94%)	
S_2	297/4.18	0.0173	298/4.16	0.0597	386/ 3.21	0.0001
S_2-cont.	HOMO-1—LUMO (77%) HOMO—LUMO (3.2%)		HOMO-1—LUMO (85%) HOMO-4—LUMO (6%)		HOMO-1—LUMO (84%) HOMO—LUMO (3.7%)	
S_3	271/4.58	0.0671	267/4.64	0.0351	361/ 3.43	0.0005
S_4	244/5.08	0.0010	247/5.02	0.0050	356/ 3.48	0.0098
S_5	340/5.17	0.0137	236/5.26	0.0182	301/ 4.17	0.1512
S_6	236/5.26	0.0009	223/5.56	0.0529	295/ 4.19	0.0819

[a] "S_1-cont." represents the orbital contribution of the S_1 state.

[b] "326/3.80" means the same value in different units, nm and eV, respectively.

[c] The data in parenthesis indicates the contribution of the transition to the corresponding excited-state.

[d] "A-DMF (S_0)" represents the equilibrium structure of ground state, the data below is its vertical electronic spectra.

[e] "A-DMF (S_1)" represents the S_1 equilibrium structure. The corresponding emission spectrum arises from the S_1 equilibrium structure of A-DMF.

Table 2. Calculated net charge distribution for different electronic states of A-DMF, together with the net charge difference of S_1 and S_0 states. The dipole moments in debye for the S_0 and S_1 states are also presented.

	S_0	S_1	Diff-S_1-S_0[a]
Dipole Moment	4.591	8.984	4.393
N1	-0.269	-0.237	0.032
H1	0.344	0.353	0.009
O1	-0.295	-0.282	0.013
O2	-0.293	-0.180	0.113
S1	0.099	0.233	0.134
C8	0.473	0.223	-0.252
C9	-0.169	-0.197	-0.028
C10	0.262	-0.311	-0.573
CT-thia.[b]			-0.552
C1	-0.773	-0.663	0.110
C2	1.552	1.533	-0.019
C3	-1.069	-0.503	0.566
C4	0.215	0.028	-0.187
C5	-0.387	0.223	0.164
C6	-0.253	-0.270	-0.017
H2	0.152	0.106	-0.046
H4	0.132	0.114	-0.018
H5	0.137	0.120	-0.017
H6	0.140	0.120	-0.020
O3	-0.311	-0.550	-0.239
H7	0.356	0.496	0.140
C7	-0.283	-0.460	-0.177
H3	0.177	0.171	-0.006
CT-aryl.[c]			0.234

[a] Diff-S_1-S_0 represents the net charge or dipole moment difference between the S_1 and S_0 states.

[b] The magnitude of charge transfer from the thiazolidinedione moiety.

[c] The magnitude of charge transfer from the aryl moiety.

Figure 1. Optimized geometric structures of the hydrogen-bonded complex A-DMF in different electronic states of S_0 and S_1. The important structural parameters are displayed. The atoms are labeled and numbered. Here, the dihedral angle (C1-C2-C7-C8) is between the thiazolidinedione and aryl rings.

Figure 2. Calculated absorption spectra for TZD-A and A-DMF: TZD-A (black dotted line); hydrogen-bonded A-DMF (red dotted line). The calculated and experimental absorption peak values are labeled by long and short vertical line, respectively. "calc" represents calculation; "exp" represents experiment.

Figure 3. Important frontier molecular orbitals of TZD-A (S_0), A-DMF (S_0) and A-DMF (S_1). (S_0) represents the equilibrium structure of ground state. (S_1) represents the S_1 equilibrium structure. HOMO represents the highest occupied molecular orbital, HOMO-1 the second highest occupied molecular orbital, and LUMO the lowest unoccupied molecular orbital. The charge changes of the electron donor and acceptor has been labeled in the picture.

Figure 4. Relative energy versus reaction coordinates of the distance of the O—H bond and the twisted dihedral angle in the S_1 state. P1: relative energy versus the O—H bond length, keeping dihedral angle=33.46°; P2: relative energy versus the O—H bond length, keeping dihedral angle=87.40°; P3: relative energy versus dihedral angle, keeping the O—H bond length at 1.409 Å；P4: relative energy versus dihedral angle, keeping the O—H bond length at 0.981 Å. Here, the dihedral angle (C1-C2-C7-C8) is between the thiazolidinedione and aryl rings. The potential curves drawn by solid and dotted lines are calculated with TDDFT and CC2 methods, respectively.

Figure 5. The initial and local minimum structures along the potential curves in Figure 4. "Pn-1" represents the initial configuration along the potential curves Pn (n=1, 2, 3, 4); "Pn-2" represents the configuration of the local minimum along the potential curves Pn (n=1, 2, 3, 4).

Figure 6. The relative energies and the important geometric structures corresponding to the local minima of the above potential curves in Figure 4. “P1-2” represents the configuration of the local minimum along the potential curve P1; “P4-2” represents the stable configuration along the potential curve P4; “P2-2 (P3-2)” represents the stable structure along the potential curve P2(P3).

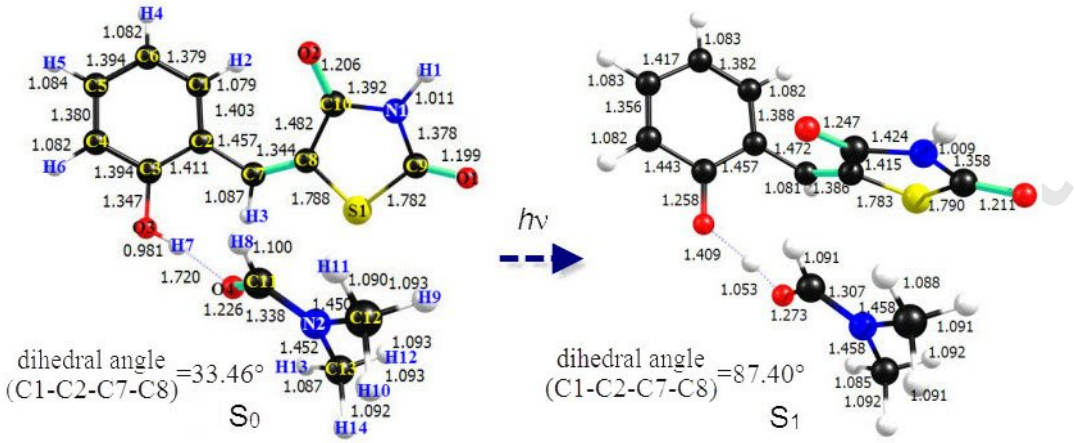

Figure 1.

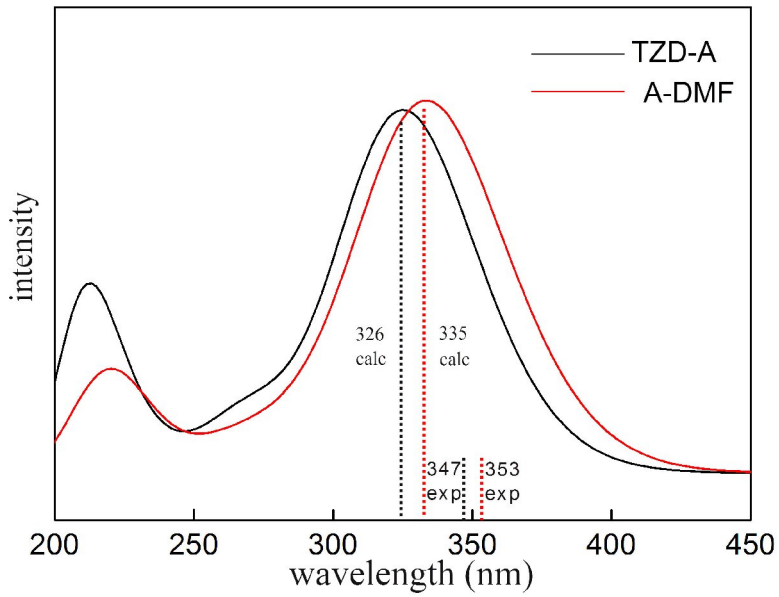

Figure 2.

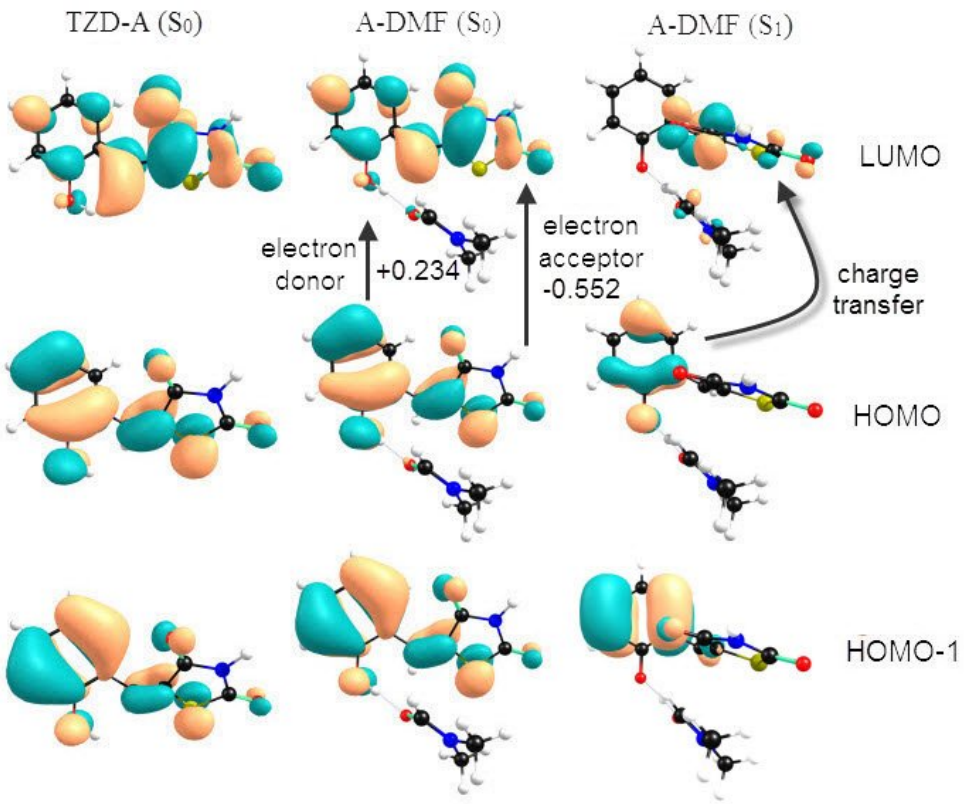

Figure 3.

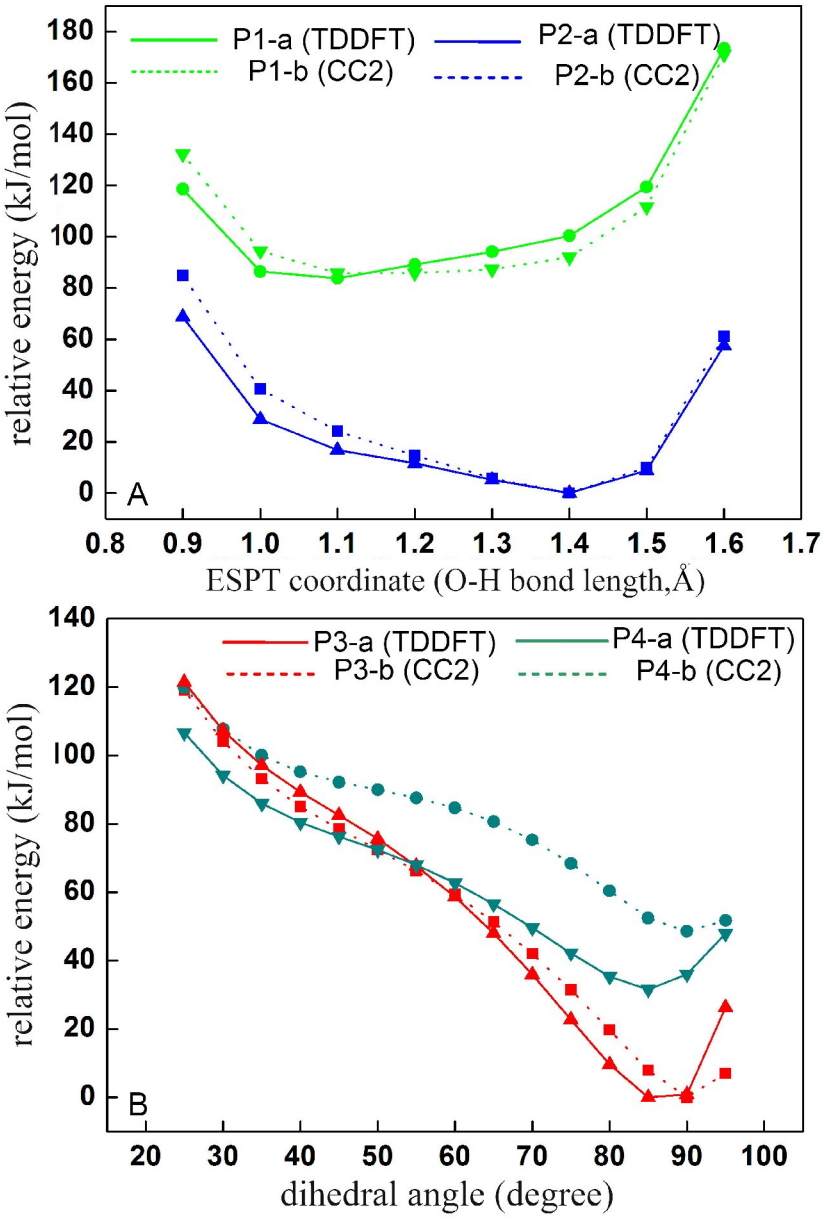

Figure 4.

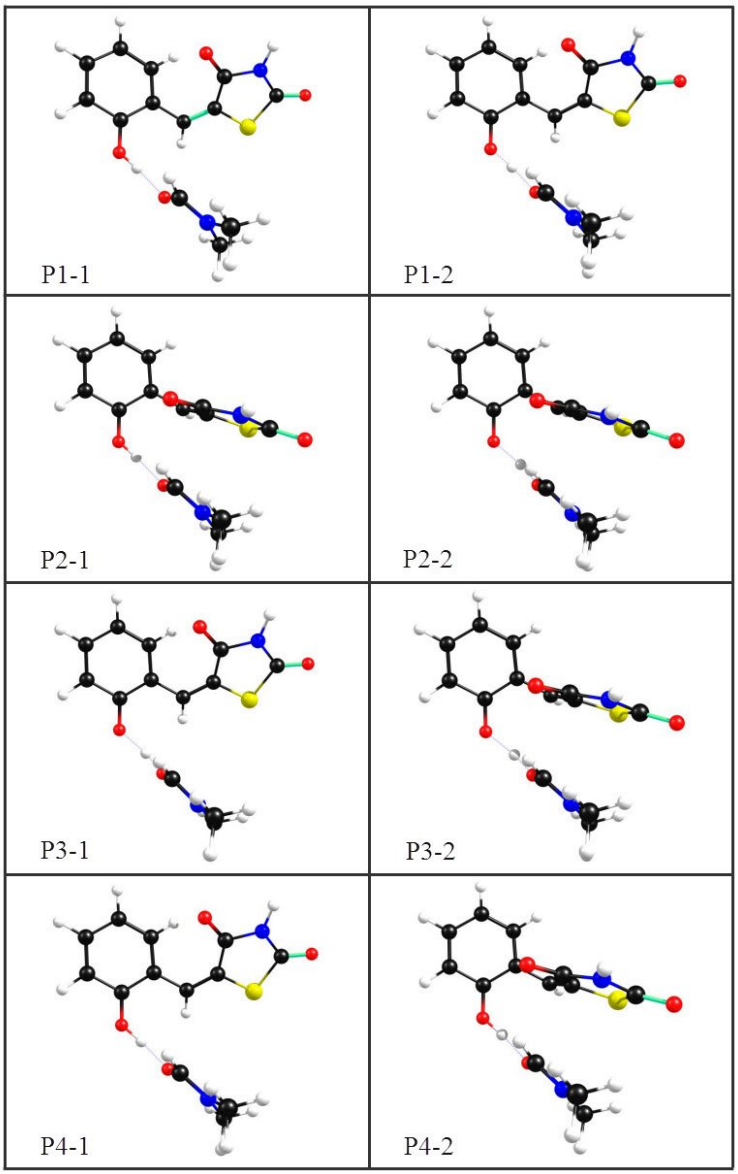

Figure 5.

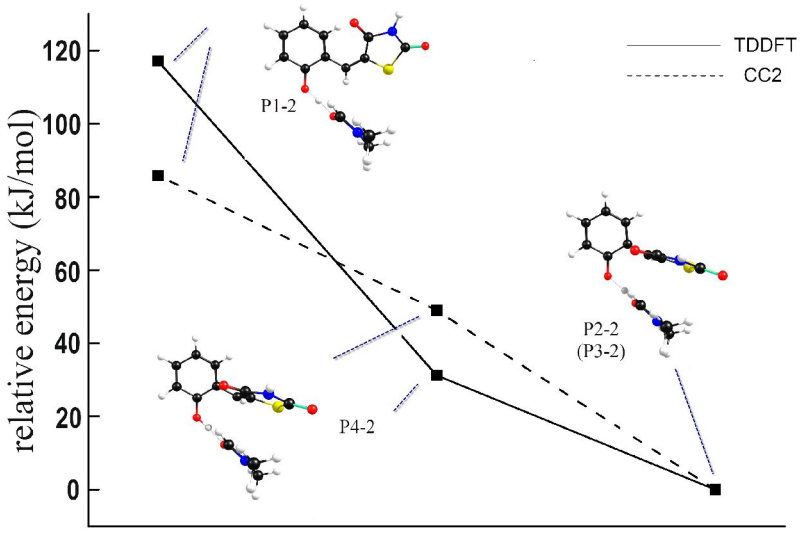

Figure 6.